New Trends and Issues Proceedings on Advances in Pure and Applied Sciences

Issue 9, (2017) 01-13

www.propaas.eu
ISSN: 2547-880X

Selected Paper of Selected Paper of 3rd Global Conference on Material Sciences (GC-MAS-2017), 28-30 August 2017
Bahcesehir University Besiktas Campus, Istanbul, Turkey

Microwave energy-based synthesis and characterisation of hollow carbon nanospheres decorated with carbon nanotubes or metal oxide nanowires

Selcuk Poyraz [a]*, Department of Chemical Engineering, Auburn University, Auburn 36849, USA: Department of Textile Engineering, Corlu Faculty of Engineering, Namik Kemal University, 59860 Corlu, Turkey
Jonathan Cook [b], Department of Chemical Engineering, Auburn University, Auburn 36849, USA
Zhen Liu [c], Department of Physics and Engineering, Frostburg State University, Frostburg 21532-2303, USA
Lin Zhang [d], Electronic Materials Research Laboratory, Key Laboratory of the Ministry of Education and International Center for Dielectric Research, Xi'an Jiaotong University, Xi'an 710049, China
Amit Nautiyal [e], Department of Chemical Engineering, Auburn University, Auburn 36849, USA
Britta Hohmann [f], Department of Chemical Engineering, Auburn University, Auburn 36849, USA
Solveig Klamt [g], Department of Chemical Engineering, Auburn University, Auburn 36849, USA
Xinyu Zhang [h], Department of Chemical Engineering, Auburn University, Auburn 36849, USA

Suggested Citation:
Poyraz, S., Cook, J., Liu, Z., Zhang, L., Nautiyal, A., Hohmann, B., Klamt, S. & Zhang, X. (2017). Microwave energy-based synthesis and characterisation of hollow carbon nanospheres decorated with carbon nanotubes or metal oxide nanowires. *New Trends and Issues Proceedings on Advances in Pure and Applied Sciences*. [Online]. 9, 01–13. Available from: www.propaas.eu

Selection and peer review u nder responsibility of Assist. Prof. Dr. Engin Baysen, Near East University, Nicosia, Cpyrus

Abstract

Hollow carbon nanospheres (HCNSs), with either carbon nanotube (CNT) or metal oxide nanowire (MONW) decoration on their surface, were synthesised as building materials with a great potential for the next generation advanced applications. A well-established, polymeric latex NS synthesis method and a simply modified version of a microwave (MW) energy-based carbonisation approach, i.e. Poptube, were systematically combined to obtain these HCNSs. Through this simple, facile, affordable and easily scalable 'combined synthesis method', it was managed to successfully produce HCNSs with an unique

* ADDRESS FOR CORRESPONDENCE: **Selcuk, Poyraz,** Department of Chemical Engineering, Auburn University, Auburn 36849, USA: Department of Textile Engineering, Corlu Faculty of Engineering, Namik Kemal University, 59860 Corlu, Turkey.
E-mail address: spoyraz@nku.edu.tr / Tel.: +1-334-844-5439; Fax: +1-334-844-4068

morphological, spectroscopic, thermal and elemental features, all of which were strongly supported by both various material characterisation test results and the relevant previous literature data. Thus, it is believed that the as-synthesised CNT or MONW decorated HCNSs (CNT–MONW/HCNS) from the above-mentioned method would soon become the materials of preference for the next generation advanced applications in various science and engineering fields.

Keywords: Hollow carbon nanospheres, carbon nanotubes, metal oxide nanowires, microwave energy, conducting polymer.

1. Introduction

Recently, bare hollow carbon spheres (HCSs) or their core–shell derivatives combining hollow and porous carbon nanostructures have received increasing attention in various fields of science and engineering such as catalysis, composites for high energy storage (supercapacitor, lithium–ion/sulfur battery (LIB), fuel cell etc.), water treatment, magnetic resonance imaging (MRI) and electromagnetic interference) shielding due to their advantageous features such as high electrochemical reactivity, low density and long-term thermo/mechanical stability. [1–8] In terms of different structure and type of materials, the core–shell concept is generally presented as core-A@shell-B in different ways, such as metal@polymer, metal@carbon, carbon@carbon and metal-oxide@carbon. [6–9] In such systems, the hollow spheres (or shell) usually act as a barrier to prevent the encapsulated or decorated nanostructures from coalescence and also provide them a vast interstitial space for their accommodation in large quantities, which is crucial to improve and optimise the overall performance of such materials in different applications.

To date, several methods have been proposed to prepare various HCS composites decorated with different nanomaterials and morphologies, [10–12] including the template-assisted methods, [13, 14] precursor-controlled carbonisation, [15] solvo/thermal methods, [16] self-assembly by using soft templates, [17] pyrolysis, [18] and chemical vapour deposition with a relevant catalyst. [19] For this purpose, polymeric materials, i.e., conducting polymers (CPs), have been commonly used as carbon precursors. [20, 21] The as-obtained HCSs from those approaches were often benefited as the electrode materials for energy storage applications via combining the advantages of nanostructured carbon materials' design and the unique electrochemical features of the decorating nanomaterials in one structure. However, since the as-prepared HCSs average diameter usually falls in the micron range, [22, 23] it causes a restriction on their total specific active surface area. [11, 24–26] Thus, in order to address the functional material needs for the above mentioned applications' vast potential and to tackle the so called size distribution problem; a simple, facile, easily scalable and low cost method needs to be urgently developed to obtain Hollow carbon nanospheres (HCNSs) with larger surface area and smaller diameters.

In this manner, along with the combination of different precursor chemicals, polypyrrole (PPy) had been commonly used as an active material to achieve superior performances in nanocomposites. [27] Among CPs, PPy has been one of the most extensively studied members due to its many advantages such as its simple and straightforward preparation at ambient conditions, low cost and high polymerisation yield, unique electrochemical properties, relatively high conductivity, and long-term thermal and environmental stability with good processability. [28, 29] Thus, throughout the last decade, various nanostructured PPy morphologies from zero dimensional (0D) nanogranules to three-dimensional (3D) sea urchin-like nanospheres have been copiously synthesised [8, 26, 30–35].

Numerous ongoing research efforts based on different types of active species, such as heteroatom containing surface functional groups, [36, 37] transition metal oxides [38, 39] and electrically CPs, have been dedicated for the emergence of promising materials to be used in the next generation energy storage applications. [40–42] Among various metal oxides, such as MnO_2, V_2O_5, and RuO_2 etc., Fe_2O_3 has attracted considerable research interest as LIB anode material due to its high theoretical specific capacity (1007 mAh g^{-1}), low cost and high abundance. [39, 43, 44] However, similar to other metal oxides, Fe_2O_3 also has its own disadvantages, like low electrical conductivity, high cost and poor cycling

stability, [45] which need to be addressed in order to optimise its electrochemical application performance.

In current study, a combined method is proposed for the first time synthesis of 'carbon or metal oxide nanostructure decorated HCNSs' through a microwave (MW) energy-based carbonisation approach, [20] which was simply modified from relevant previous studies, [8, 35, 46] as shown in Figure 1. This approach can be considered more beneficial than the primarily mentioned available methods from many aspects with respect to: (i) its high efficiency, selective heating mechanism, simple experimental conditions and instrument setups; (ii) its general route, which is template-free and enables the decoration of various functional nanostructures, i.e. carbon nanotube (CNTs) and metal oxide nanowires (MONWs), on the surface of the as-obtained HCNSs; (iii) its way of using CPs as a functional carbon scaffold to provide high environmental stability and electrochemical activity for the composite structure; (iv) its versatility that allows working with different precursors; (v) its possibility to control the uniformity of the nanostructures' radial growth, and mostly importantly; (vi) its ultrafast nature to obtain 3D nanomaterials in a composite form.

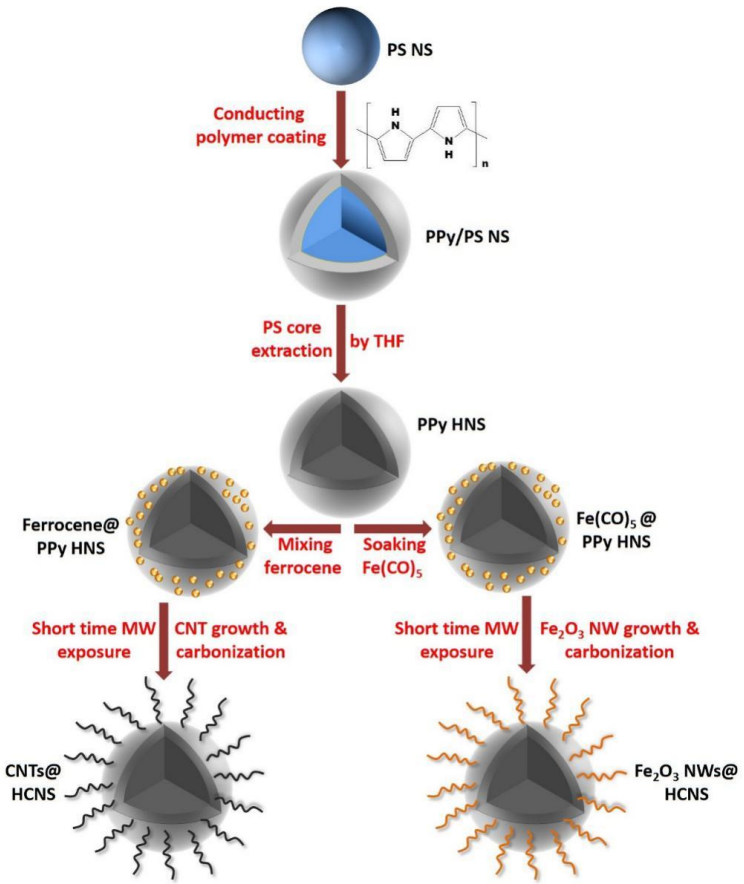

Figure 1. Schematic illustration of the CNT–MONW/HCNS composites' formation

2. Materials and methods

2.1. Materials

Following chemicals and reagents, including styrene (99%), ammonium peroxydisulfate (APS, $(NH_4)_2S_2O_8$, 98% min.), ferrocene (99%) and pyrrole (98+%) were all purchased from Alfa Aesar and used for the synthesis reactions. Sodium dodecyl sulfate (SDS, $C_{12}H_{25}NaO_4S$, 99%) was purchased from IBI Scientific. Iron pentacarbonyl ($Fe(CO)_5$, 99.5% and 99%–Fe) was purchased from Strem Chemicals.

Ethanol (EtOH, absolute 200 proof) was purchased from Electron Microscopy Sciences. Tetrahydrofuran (THF) was purchased from BDH. All reagents were used as-received without further treatment unless otherwise specified.

2.2. One-step synthesis of polystyrene latex NSs (PS NSs)

The PS NSs were prepared based on a previously reported method (H. Zhenxing *et al.*, *Eur. Polym. J.*, vol. 47, 24–30, 2011) by initially adding 4 mL of styrene monomer into a 250 mL round bottom flask containing a magnetic stir bar and 80 mL of 3 mM aq. SDS. A reflux condenser was attached to the reaction medium and the flask was placed in a preheated oil bath at 70ºC for 20 minutes under high magnetic stir. In the end, the oxidant APS was dissolved in 1 mL H_2O and slowly added into the monomer dispersion. The polymerisation reaction was allowed to proceed for 4 hours at 70ºC until yielding a milky suspension. The resulting PS NSs' latex was removed from the heat and allowed to naturally cool down to room temperature before being transferred into a container for storage purposes.

2.3. One-step synthesis of PPy coated PS NSs (PPy/PS NSs)

The as-obtained PS NSs from the previous step were used as substrates, without further purification, to coat conducting PPy on their surfaces via an in-situ oxidative polymerisation reaction at ambient conditions. Here, in a 100 mL beaker containing 60 mL 1 M aq. HCl, 10 g of PS latex was mixed with 1 mL pyrrole monomer. The solution was stirred for 10 minutes to allow homogenous distribution of monomers in the solution. The reaction medium was then moved into an ice bath where it was approximately cooled down to 5ºC. The oxidant solution was prepared by firstly dissolving 1.15 g of APS in 10 mL 1 M aq. HCl, then cooling the solution down to 5ºC, and then adding it dropwise into the monomer solution over 10 minutes under high magnetic stirring. Once the oxidant had been completely added, the reaction was left to proceed for 1 hour. The resulting black suspension was first filtered and washed with excess 1 M aq. HCl to remove any unreacted monomer and/or oxidant, and eventually it was dried overnight under vacuum at 60ºC to yield a fine black PPy/PS powder.

2.4. Preparation of hollow PPy NSs (PPy HNSs)

The PS latex cores of PPy/PS NSs were removed by using THF via subsequent carbonisation/extraction steps. Here, 5 g of PPy/PS sample was placed in a 20 mL scintillation vial with a loosely attached cap, and then exposed to 1250 W MW power for 10 seconds to minimally carbonise the PPy coating. This step helps maintaining the samples' spherical shape when their PS core are removed. The carbonised NSs were then mixed with 50 mL THF for 30 minutes at high magnetic stir to remove their PS cores. The etched NSs were collected by filtration and washed with excess THF to remove any PS traces, and finally dried under vacuum at 60ºC.

2.5. Preparation of CNT or MONW decorated hollow carbon NSs (CNT-MONW/HCNSs) via rapid MW irradiation

To obtain the CNT decorated samples: 50 mg of partially carbonised PPy HNS powder was mixed with ferrocene, which was pre-dissolved in 5 mL EtOH, at 1:1 ratio by using a speed mixer at 3500 rpm. Here, the purpose was to facilitate the penetration of dissolved ferrocene into PPy HNSs. After the evaporation of EtOH from this mixture, ferrocene formed an orange colour layer on the surface of dark PPy powder. This solid-state mixture was transferred into a capped glass vial, which was placed into a standard kitchen MW oven (Panasonic Inverter, NN-SN936B) chamber. At 1250 W MW power for 30 seconds the sample was irradiated. Upon rapid heat gain through the PPy HNSs; (i) complete carbonisation of PPy HNSs was occurred while (ii) ferrocene got rapidly decomposed and

simultaneously formed a gaseous phase, which lead (iii) to the formation/decoration of CNTs, along with continuous sparking on the sample surface. Eventually, the vial was taken out from the MW to cool down to room temperature. The as-obtained sample was collected and stored for further characterisation steps.

Similarly, to the above mentioned system, in order to obtain the MONW decorated samples; the same amount of partially carbonised PPy HNS powder was placed in a glass vial and soaked with $Fe(CO)_5$ until its surface was completely covered with the chemical (0.1 mL). After the partial evaporation of the liquid phase, the sample was placed in the MW oven chamber for the quick heating process. During 30 seconds of process time, there were vigorous sparking and glowing observed on the sample surface. Finally, after the vial was taken out and cooled down to room temperature, HCNSs with homogenous iron oxide NW decoration on their surface were gently collected from the vial bottom with a steel spatula and stored for further characterisations.

2.6. Characterisation of the as-obtained nanocomposites

Different characterisation techniques were used in order to identify the as-obtained CNT–MONW/HCNS nanocomposites' properties. Both the morphological and compositional features of these nanocomposites were analysed by JEOL JSM-7000F scanning electron microscope (SEM) equipped with an energy-dispersive X-ray (EDX) detector. Moreover, the in-depth morphological analysis of the as-obtained nanocomposites was performed on a JEOL 2100F transmission electron microscope (TEM) that was operated at 200 kV. The major functional groups exist in these nanocomposites were detected by using a Thermo Nicolet 6700 Fourier Transform Infra-Red (FT-IR) spectroscope. The as-obtained nanocomposites' thermal stability was characterised by using thermal gravimetric analysis (TGA) performed on a TA Q2000 system from room temperature up to 800°C (at 10°C/minute heating rate, in O_2 atmosphere). Additionally, the nature of the as-formed MONWs on HCNSs was determined by X-Ray diffractometry (XRD) analysis, which was performed on a Rigaku powder XRD instrument.

3. Results and Discussion

For the above-mentioned synthesis reactions, the as-used APS amount was varied to reveal its effect on the as-obtained NSs' size dependency (Figure 2, Table 1). After these PS latex NS samples were coated with PPy, their diameter values were increased ~ 20 nm (100 nm, 170 nm and 440 nm, respectively). Here, the largest PS NSs were used as templates to prepare the PPy HNSs [Figure 3 (a)]. As can be seen from Figure 3, the PPy HNSs were prepared by first, applying short-term MW energy for both partial surface carbonisation and to retain the spherical morphology during the subsequent extraction step, and then applying THF extraction to these partially carbonised samples [Figure 3 (b) and 3 (c)]. Since their PS cores were removed under high magnetic stirring, such HNSs seem like vacuumed from one side [Figure 3 (d)]. The resulting PPy HNSs from 100 nm and 170 nm samples appeared as fine black powders after the removal of their PS cores and drying. However, the ones obtained from 440 nm samples exhibited an angle dependent colour shift; transitioning from yellowish brown (when viewed from above) to a deep blue-green (when viewed from the side). This phenomenon was a result of Tyndall scattering, in which, the light interacting with particles similar in size to the wavelength causes scattering of the shorter wavelengths. Here, the 100 nm and 170 nm samples were most likely too small to produce an observable light scattering since they were much below the range of visible light wavelengths. Thus, Tyndall scattering is responsible for the opalescent property in 440 nm samples, and is desirable for materials used in photonic crystal and tunable optoelectronic applications.

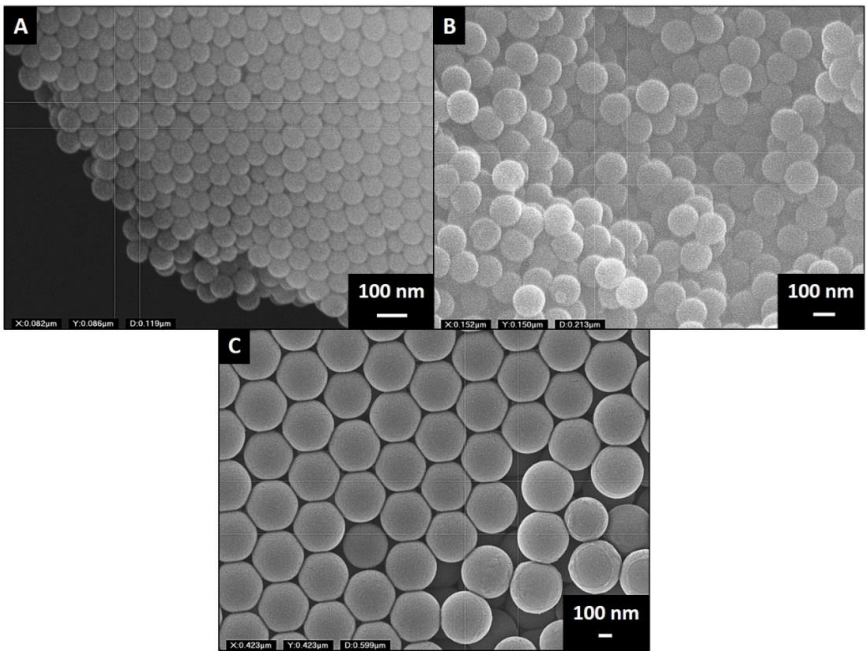

Figure 2. SEM images of the as-synthesized PS NSs with varied amounts. (a) 100 mg. (b) 68 mg. (c) 34 mg of APS, respectively.

Table 1. Summary of the as-obtained PS NSs' average diameter values with varying APS amounts

APS amount (mg)	PS NS diameter (nm)
100	~ 80
68	150
34	420

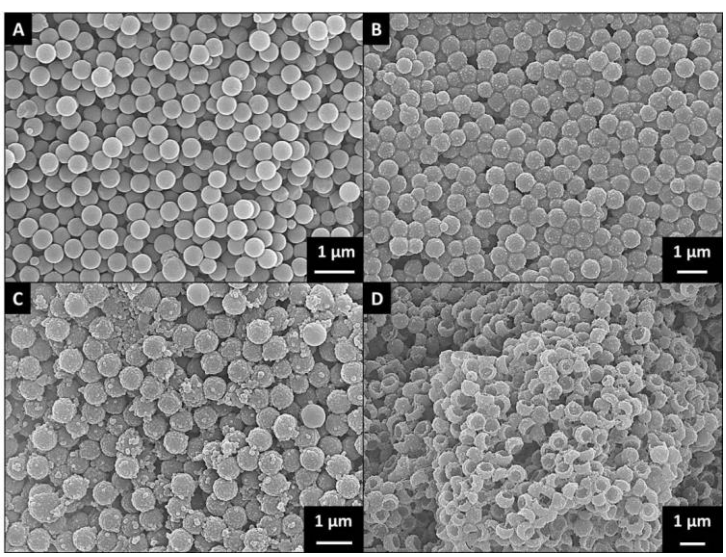

Figure 3. SEM images of (a) PS NSs. (b) PPy/PS NSs. (c) partially carbonised PPy/PS NSs. (d) PPy HNSs after THF extraction.

The as-prepared CNT–MONW/HCNS samples' morphological features were characterised by using electron microscopy techniques and the results are presented in Figures 4 and 5, respectively.

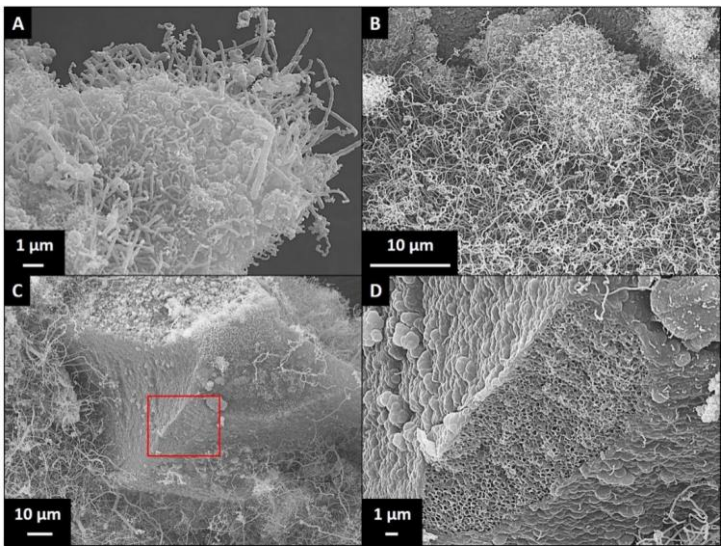

Figure 4. SEM images of (a) CNT/HCNSs. (b, c) MONW/HCNSs. (d) Detailed view of the marked area in Figure 4 (c).

SEM image of the CNT/HCNSs sample that was prepared through short-term MW energy-based Poptube approach is shown in Figure 4 (a). Based on the initial analysis of this image, it can be observed that micron long, bamboo shoot or earthworm-like [34, 47] CNTs were successfully grown at carbonised HNSs' cluster surface. In addition, the as-grown CNTs' coverage density is seemed to be very homogenous, which is a crucial factor for the future application performance of this sample. In Figures 4 (b) and 4 (c), the as-prepared MONW/HCNS composites' overall morphology are exhibited. Compared to the CNT/HCNS sample, the spaghetti-like MONWs grown at the HCNS cluster surface are much longer and their surface coverage is much denser, as well. In Figure 4 (d), detailed view of the MONW decorated HCNSs exist in the cluster can be clearly observed. Such nanocomposite structures can be effectively used for both water treatment and energy storage applications with respect to their ultra-high specific active surface area that is supported by the as-grown microns long iron oxide NWs [8].

The in-depth morphological analyses of the as-prepared samples were done by using TEM imaging technique. Expectedly, the results presented in Figure 5 are in good agreement with the ones obtained from SEM characterisation. PPy/PS NSs can be seen in Figure 5 (a). These NSs have a pretty uniform size distribution that ranges between 600 and 650 nm. PPy nanogranule clusters, which were composed of nanogranules with ~ 50 nm average diameter, covering these NSs' surface can be also observed from this Figure. PPy HNSs with ~ 600 nm average diameter can be observed in Figure 5 (b). The dense PPy coverage at these HNSs' surface is also obvious in this Figure. CNT decorated and carbonised versions of the same HNSs can be seen in Figure 5 (c). Some of both the HCNSs and CNTs decorating their surface were broken probably because of the ultrasonication-based sample preparation step applied before TEM imaging. A supporting proof for this phenomenon is shown in Figure 5 (d), in which, a broken HCNS with another broken, tip-grown CNT with secondary growths at its hollow stem can be clearly seen. Based on the measurements taken from this Figure it can observed that: (i) the broken HCNS is ~ 600 nm in diameter, (ii) the broken CNT has ~ 2 µm long hollow stem with (iii) ~ 50 nm earthworm-like secondary CNT growths on it and (iv) CNTs encapsulated iron nanoparticle (NP) tip is ~ 270 nm in diameter. These results are also strongly supported by the ones obtained from the relevant previous studies, as well. [26, 34, 47–49] Differently from their CNT/HCNS equivalents, MONW/HCNS composite samples were observed to have tiny core–shell NP decoration

on their surface rather than MONWs. Such NPs were made up of Fe_2O_3 cores that were encapsulated within the graphitised carbon shells. The reason of this situation is believed to be simply related with the disintegration of microns long, web-like MONWs into its constituents, most probably by the above-mentioned ultrasonication-based sample preparation process. This result agrees well with the ones from the relevant previous studies, in which, the NWs obtained from $Fe(CO)_5$ do not have solid and continuous structures. Instead, these NWs exhibit a pearl necklace-like morphology that is composed of adjacent NPs encapsulated within graphitised carbon layers. [8, 26, 35, 50, 51] Based on the measurements taken, such NPs' diameter size distribution ranges between 30–100 nm.

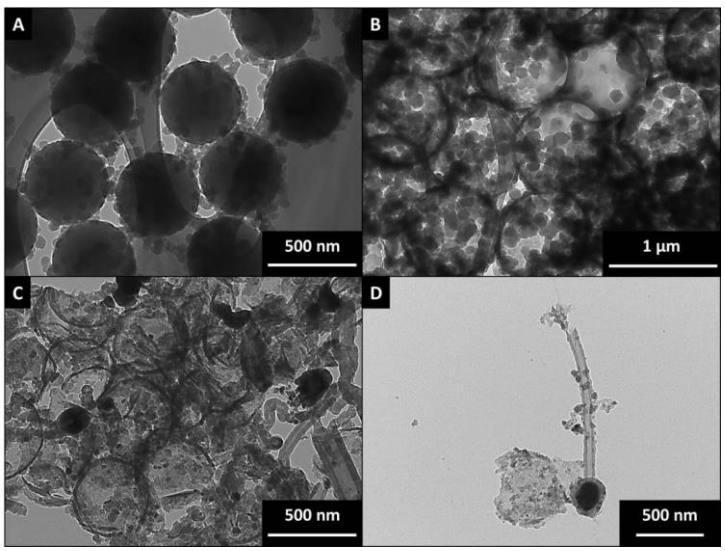

Figure 5. TEM images of (a) PPy/PS NSs. (b) PPy HNSs. (c) CNT/HCNS. (d) A broken, tip-grown, single CNT with secondary growths at its hollow stem and the encapsulated Fe NP at its tip, and a broken HCNS with carbonised PPy nanogranules at its surface.

After the morphological property characterisation of the as-prepared MONW/HCNS composite was completed, its elemental composition was also investigated by using EDX analysis. According to the results shown in Figure 6 and Table 2, it is obvious that the as-grown MONWs at HCNSs' surface are made up of Fe and O elements.

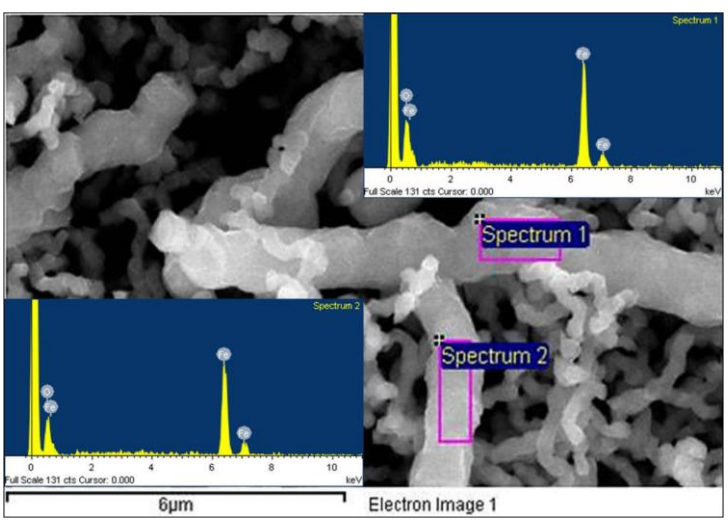

Figure 6. EDX results of the MONWs obtained from Fe $(CO)_5$ system

Table 2. Summary of the EDX results shown in Figure 6

Spectrum	Fe (wt%)	O (wt%)	Total
1	67.47	32.53	100
2	58.32	41.68	100

Additionally, in order to identify these MONWs' crystalline nature, XRD analysis was performed on the relevant sample. It can be observed in Figure 7 that characteristic diffraction peaks appeared on the as-grown MONW's spectrum was matching with the standard Fe_2O_3 hematite (JCPDS: 33-0664) [8, 26].

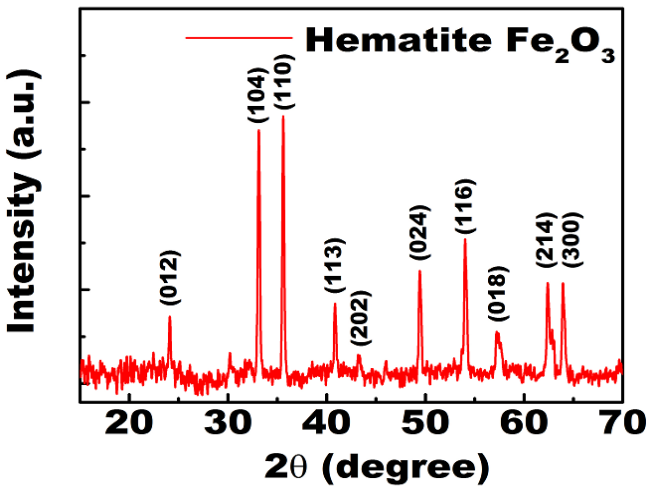

Figure 7. X-Ray diffractogram of the as-grown MONWs in MONW/HCNS sample

Last but not the least, the major functional groups' verification and thermal stability analysis of the as-synthesised NSs were conducted by using FT-IR and TGA characterisations, respectively. The FT-IR results shown in Figure 8 and summarised in Table 3, indicate that PPy/PS NS sample was successfully synthesised in a hybrid nanocomposite form and exhibited both of its components' characteristic peaks, which were already presented in relevant previous literature [22, 29].

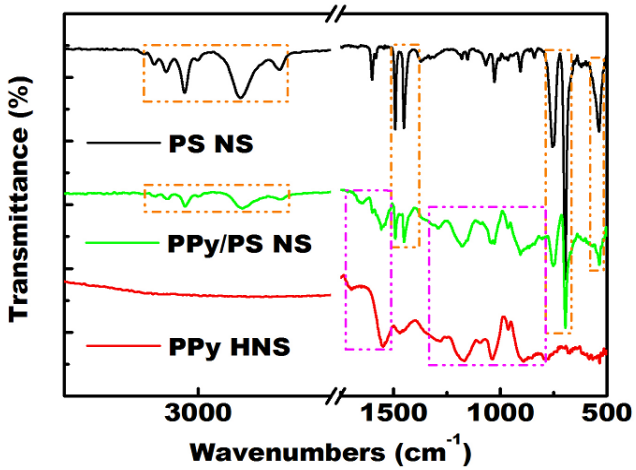

Figure 8. FT-IR spectra of the as-synthesised PS NS, PPy/PS NS and PPy HNS samples

Table 3. Summary of the common FT-IR spectra peaks detected in PS/PPy NS sample shown in Figure 8

Peak's origin	Wavenumber (cm^{-1})	Definition
From PS	3080, 3055, 3025	aromatic = C-H stretching vibrations
	2920, 2850	alkyl C-H stretching vibrations
	1490, 1450	aromatic – C = C – stretching vibrations
	755	aromatic = C-H out-of-plane deformation vibrations
	700, 535	out-of-plane ring deformation vibrations
From PPy	1555	secondary amine N-H peak of pyrrole ring
	1470	aromatic C-N stretching of pyrrole ring
	1290	$C\text{-}N^{+}$-H stretching vibrations in pyrrole ring
	1190	C-H in-plane vibrations
	1075	N-H in-plane vibrations (doped state PPy presence)
	905	C-H out-of-plane vibrations

The PPy/PS NS sample's thermal features also exhibited both of its components' characteristics as can be seen on its TGA thermogram shown in Figure 9. As indicated by the first purple circle, up to 225°C, this sample went through ~ 2.5% weight loss, which was caused by the removal of moisture content, the dopants and the low molecular weight heteroatoms, respectively, from its PPy component. The next two orange circles between 325°C and 425°C indicate the second major weight loss (78%) occurred in PPy/PS NS sample, which was caused by the thermal decomposition of this sample's PS component. The last ~ 14.4% weight loss, occurred between 425°C and 600°C, indicates the completion of PPy content's thermal decomposition (purple circle) in this sample.

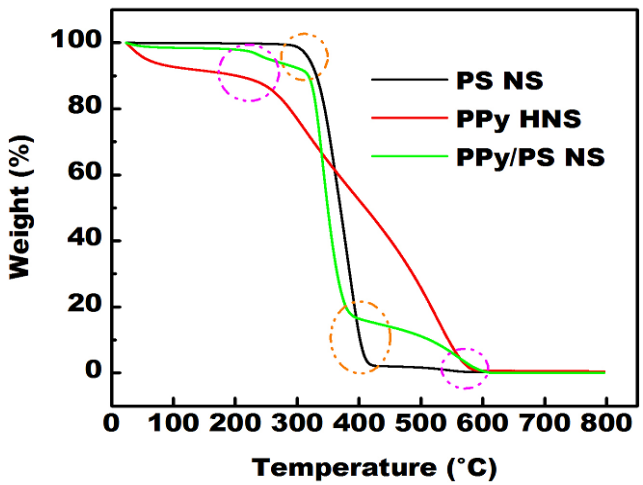

Figure 9. TGA thermograms of the as-synthesised PS NS, PPy/PS NS and PPy HNS samples

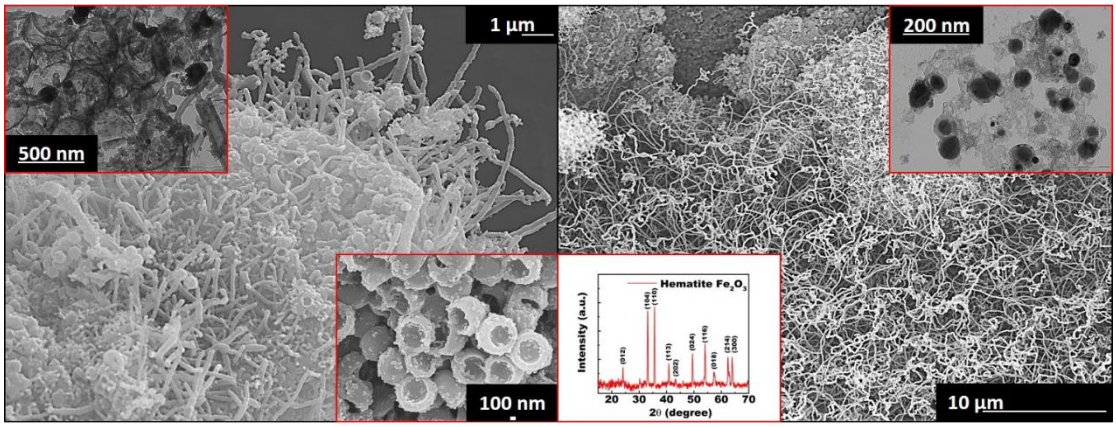

Figure 10.Table of contents artwork

4. Conclusion

The following aspects can be listed as the particular interest of this study: (i) conducting well-established and cutting-edge experimental studies, preferably with the previous literature verification, to build a theory that unveils the structure-property relationship in novel HCNS composites; (ii) development of new multifunctional composite materials for engineering applications with a vast potential; (iii) characterisation of the structure and chemistry of the as-obtained nanocomposite materials to understand their various features; and (iv) elucidation of the efficient mechanisms involved in the synthesis and processing of the next-generation nanocomposites as a route to determine their applications.

Thus, according to these interests, the first time synthesis of CNT or MONW decorated HCNSs was achieved throughout this study. Two well-established methods, namely polymeric latex NS synthesis and MW energy-based Poptube, were combined for the success of this approach, which is strongly supported by both various material characterisation test results and relevant previous literature data. Besides, the as-synthesised HCNS composites through this approach are more advantageous than the previously presented ones in the literature, with respect to; (i) their simple, facile, easily scalable and low cost combined synthesis method and (ii) their enhanced application performance along with the presence of CNT and MONW decorations on their surface, which provide ultra-high specific active surface area. In conclusion, it is believed that the as-obtained CNT-MONW/HCNS composites will soon become the materials of preference for various advanced applications such as energy harvesting/storage, MRI, water treatment and drug delivery.

Acknowledgments

The authors gratefully acknowledge the financial support from Namik Kemal University scientific research award NKUBAP.00.17.AR.15.04.

References

[1] X. W. Lou *et al.*, “Hollow micro-/nanostructures: synthesis and applications,” *Adv. Mater.*, vol. 20, pp. 3987–4019, 2008.

[2] M. Kim *et al.*, “Synthesis of nanorattles composed of gold nanoparticles encapsulated in mesoporous carbon and polymer shells,” *Nano Lett.*, vol. 2, 1383–1387, 2002.

[3] K. Kamata *et al.*, “Synthesis and characterization of monodispersed core−shell spherical colloids with movable cores,” *J. Am. Chem. Soc.*, vol. 125, pp. 2384–2385, 2003.

[4] N. Liu *et al.*, "A yolk-shell design for stabilized and scalable li-ion battery alloy anodesvol," *Nano Lett.*, vol. 12, pp. 3315–3321, 2012.
[5] G. Y. Zheng *et al.*, "Amphiphilic surface modification of hollow carbon nanofibers for improved cycle life of lithium sulfur batteries," *Nano Lett.*, vol. 13, pp. 1265–1270, 2013.
[6] S. Ikeda *et al.*, *Angewandte Chemie-International Edition*, vol. 45, pp. 7063–7066, 2006.
[7] W. M. Zhang *et al.*, "Tin-nanoparticles encapsulated in elastic hollow carbon spheres for high-performance anode material in lithium-ion batteries," *Adv. Mater.*, vol. 20, pp. 1160–1165, 2008.
[8] Z. Liu *et al.*, "Ultrafast Cr (VI) removal from polluted water by microwave synthesized iron oxide submicron wires," *Chem. Commun.*, vol. 50, pp. 8036–8039, 2014.
[9] A. B. Fuertes *et al.*, "Synthetic route to nanocomposites made up of inorganic nanoparticles confined within a hollow mesoporous carbon shell," *Chem. Mater*., vol. 19, pp. 5418–5423, 2007.
[10] N. Jayaprakash *et al.*, *Angewandte Chemie-International Edition*, vol. 50, pp. 5904–5908, 2011.
[11] S. B. Yang *et al.*, *Adv. Mater.*, vol. 22, pp. 838–842, 2010.
[12] C. F. Zhang *et al.*, *Angewandte Chemie-International Edition*, vol. 51, pp. 9592–9595, 2012.
[13] F. Caruso *et al.*, "Magnetic nanocomposite particles and hollow spheres constructed by a sequential layering approach," *Chem. Mater*., vol. 13, pp. 109–116, 2001.
[14] J. Jang and H. Ha, "Fabrication of carbon nanocapsules using PMMA/PDVB core/shell nanoparticles," *Chem. Mater*., vol. 15, pp. 2109–2111, 2003.
[15] A. H. Lu *et al.*, "Easy synthesis of hollow polymer, carbon, and graphitized microspheres," *Angew. Chem. Int. Edit.*, vol. 49, pp. 1615–1618, 2010.
[16] Z. F. Wang *et al.*, *Carbon*, vol. 44, pp. 3277–3284, 2006.
[17] S. Z. Qiao *et al.*, "Surface-functionalized periodic mesoporous organosilica hollow spheres," *J. Phys. Chem. C*, vol. 113, pp. 8673–8682, 2009.
[18] L. Q. Xu *et al.*, *Carbon*, vol. 43, pp. 1090–1092, 2005.
[19] N. A. Katcho *et al.*, "Carbon hollow nanospheres from chlorination of ferrocene," *Chem. Mater*., vol. 19, pp. 2304–2309, 2007.
[20] X. Y. Zhang and S. K. Manohar, *Chem. Commun.*, vol. 23, pp. 2477–2479, 2006.
[21] S. Fujii *et al.*, "One-pot synthesis of conducting polymer-coated latex particles: ammonium persulfate as free radical initiator and chemical oxidant," *Chem. Commun*., vol. 46, pp. 7217–7219, 2010.
[22] J. R. Zhang *et al.*, "Simple synthesis of polypyrrole-polystyrene hybrid hollow spheres," *Mater. Chem. Phys.*, vol. 134, pp. 1072–1078, 2012.
[23] C. H. Chang *et al.*, *J. Nanomater.*, vol. 168025, pp. 1–6, 2010.
[24] J. W. Fu *et al.*, "Controlled fabrication of uniform hollow core porous shell carbon spheres by the pyrolysis of core/shell polystyrene/cross-linked polyphosphazene composites," *Chem. Commun.*, vol. 46, pp. 6563–6565, 2010.
[25] B. Fang *et al.*, "Fabrication of hollow core carbon spheres with hierarchical nanoarchitecture for ultrahigh electrical charge storage," J. Mater. Chem., vol. 22, pp. 19031–19038, 2012.
[26] Z. Liu *et al.*, "An ultrafast microwave approach towards multi-component and multi-dimensional nanomaterials," *RSC Adv.*, vol. 4, pp. 9308–9313, 2014.
[27] S. Fujii *et al.*, "Synthesis and characterization of polypyrrole−palladium nanocomposite-coated latex particles and their use as a catalyst for suzuki coupling reaction in aqueous media," *Langmuir*, vol. 26, pp. 6230–6239, 2010.
[28] A. Malinauskas *et al.*, "Chemical deposition of conducting polymers," *Polym.*, vol. 42, pp. 3957–3972, 2001.
[29] S. H. Cho *et al.*, "Synthesis of nano-sized polypyrrole-coated polystyrene latexes," *Colloid. Surface. A*, vol. 255, pp. 79–83, 2005.
[30] Z. Liu *et al.*, "Green-nano approach to nanostructured polypyrrole," *Chem. Commun.*, vol. 47, pp. 4421–4423, 2011.
[31] X. Y. Zhang and S. K. Manohar, "Bulk Synthesis of Polypyrrole Nanofibers by a Seeding Approach," *J. Am. Chem. Soc.*, vol. 126, pp. 12714–12715, 2004.
[32] X. Y. Zhang & S. K. Manohar, "Narrow pore-diameter polypyrrole nanotubes," *J. Am. Chem. Soc.*, vol. 127, pp. 14156–14157, 2005.

[33] Z. Liu *et al.*, "Oxidative template for conducting polymer nanoclips," *J. Am. Chem. Soc.*, vol. 132, pp. 13158–13159, 2010.

[34] Z. Liu *et al.*, "Poptube approach for ultrafast carbon nanotube growth," *Chem. Commun.*, vol. 47, pp. 9912–9914, 2011.

[35] X. Y. Zhang & Z. Liu, "Recent advances in microwave initiated synthesis of nanocarbon materials," *Nanoscale*, vol. 4, pp. 707–714, 2012.

[36] D. Hulicova *et al.*, "Electrochemical performance of nitrogen-enriched carbons in aqueous and non-aqueous supercapacitors," *Chem. Mater.*, vol. 18, pp. 2318–2326, 2006.

[37] Z. Liu *et al.*, "Conducting polymer - metal nanocomposites synthesis and their sensory applications," *Curr. Org. Chem.*, vol. 17, pp. 2256–2267, 2013.

[38] C. C. Hu *et al.*, "Design and tailoring of the nanotubular arrayed architecture of hydrous ruo2 for next generation supercapacitors," *Nano Lett.*, vol. 6, pp. 2690–2695, 2006.

[39] L. L. Zhang *et al.*, "Enhancement of electrochemical performance of macroporous carbon by surface coating of polyaniline," *Chem. Mater.*, vol. 22, pp. 1195–1202, 2010.

[40] T. L. Kelly *et al.*, "Supercapacitive properties of PEDOT and carbon colloidal microspheres," *ACS Appl. Mater. Interfaces*, vol. 1, pp. 2536–2543, 2009.

[41] Z. B. Lei *et al.*, "Growth of polyaniline on h**o**llow carbon spheres for enhancing electro capacitance," *J. Phys. Chem. C*, vol. 114, pp. 19867–19874, 2010.

[42] Z. Chen *et al.*, "Design and synthesis of hierarchical nanowire composites for electrochemical energy storage," *Adv. Funct. Mater.*, vol. 19, pp. 3420–3426, 2009.

[43] S. B. Yang *et al.*, "Fabrication of graphene-encapsulated oxide nanoparticles: towards high-performance anode materials for lithium storage," *Angew. Chem. Int. Ed.*, vol. 49, 8408–8411, 2010.

[44] X. Y. Lai *et al.*, "Recent advances in micro-/nano-structured hollow spheres for energy applications: from simple to complex systems,**"** *Energy Environ. Sci.***,** vol. 5, pp. 5604–5618, 2012.

[45] L. T. Kang *et al.*, "One-step combustion synthesis of CNTs doped Fe2O3/C nanocomposites as electrode materials for supercapacitors," *Fuller. Nanotub. Car. N*, vol. 23, pp. 715–720, 2015.

[46] E. Raymundo-Pinero *et al.*, "Tuning carbon materials for supercapacitors by direct pyrolysis of seaweeds," *Adv. Funct. Mater.*, vol. 19, 1032–1039, 2009.

[47] S. Poyraz *et al.*, "Ultrafast microwave welding/reinforcing approach at the interface of thermoplastic materials," *ACS Appl. Mater. Interfaces*, vol. 7, pp. 22469–22477, 2015.

[48] S. Poyraz *et al.*, "Devulcanization of scrap ground tire rubber and successive carbon nanotube growth by microwave irradiation," *Curr. Org. Chem.*, vol. 17, pp. 2243–2248, 2013.

[49] H. Xie *et al.*, "Microwave-assisted fabrication of carbon nanotubes decorated polymeric nano-medical platforms for simultaneous drug delivery and magnetic resonance imaging," *RSC Adv.*, vol. 4, pp. 5649–5652, 2014.

[50] Z. Liu *et al.*, *Sci. Rep.* vol. 6, pp. 22503–22510, 2016.

[51] A. M. Schwenke *et al.*, "Synthesis and modification of carbon nanomaterials utilizing microwave heating," *Adv. Mater.*, vol. 27, pp. 4113–4141, 2015.